A narrow ear canal reduces sound velocity to create additional acoustic inputs in a microscale insect ear

Daniel Veitch[a,1], Emine Celiker[a,1,2], Sarah Aldridge[a], Christian Pulver[a], Carl D. Soulsbury[a], Thorin Jonsson[b], Charlie Woodrow[a], and Fernando Montealegre-Z[a,2]

[a]School of Life Sciences, Joseph Banks Laboratories, University of Lincoln, Lincoln LN6 7TS, United Kingdom; and [b]Institute of Biology, Universitätsplatz 2, Karl-Franzens-University Graz, 8010 Graz, Austria

Edited by David A. Weitz, Harvard University, Cambridge, MA, and approved January 24, 2021 (received for review August 14, 2020)

Located in the forelegs, katydid ears are unique among arthropods in having outer, middle, and inner components, analogous to the mammalian ear. Unlike mammals, sound is received externally via two tympanic membranes in each ear and internally via a narrow ear canal (EC) derived from the respiratory tracheal system. Inside the EC, sound travels slower than in free air, causing temporal and pressure differences between external and internal inputs. The delay was suspected to arise as a consequence of the narrowing EC geometry. If true, a reduction in sound velocity should persist independently of the gas composition in the EC (e.g., air, CO_2). Integrating laser Doppler vibrometry, microcomputed tomography, and numerical analysis on precise three-dimensional geometries of each experimental animal EC, we demonstrate that the narrowing radius of the EC is the main factor reducing sound velocity. Both experimental and numerical data also show that sound velocity is reduced further when excess CO_2 fills the EC. Likewise, the EC bifurcates at the tympanal level (one branch for each tympanic membrane), creating two additional narrow internal sound paths and imposing different sound velocities for each tympanic membrane. Therefore, external and internal inputs total to four sound paths for each ear (only one for the human ear). Research paths and implication of findings in avian directional hearing are discussed.

bioacoustics | katydid hearing | sound propagation | finite element analysis

Tetrapod auditory perception is based on sound capturing, transformation of airborne vibrations into fluid vibrations, and mechanical frequency decomposition followed by the transduction of the mechanical energy into electrochemical signals by the auditory receptor neurons (1). Adaptations for the first step—the efficient capture of the sound waves—vary across taxa and have evolved independently in mammals, reptiles, and birds (2, 3). In terrestrial mammals, for instance, sound capture involves the pinna and the ear canal (EC), which vary in morphology depending on a species' hearing abilities (4). The symmetrical arrangement, topology, and spatial distribution of the components of the outer ear create an asymmetrical orientation relative to a potential sound source, enhancing directional hearing acuity.

An analogue mechanism of hearing has been reported in katydids (bush crickets; Orthoptera, Tettigoniidae), which also exhibit the three basic steps of hearing reported in mammals (5). These insects use hearing for social communication (e.g., finding a mate) (5) and predator detection (6–8), both of which require precise auditory perception and orientation. Different from tetrapods, the katydid ear, also known as the tympanal organ, is located in the foretibia (8). Each ear possesses two tympanic membranes (TMs), called the anterior tympanic membrane (ATM) and the posterior tympanic membrane (PTM) (9, 10). Both ATM and PTM are exposed to airborne sound arriving externally to the legs, but they are also backed internally by an air-filled pipe, the acoustic trachea, which is derived from the insect's respiratory system and opens in a large spiracle at the side of the thorax (8, 11, 12). Sound travels into the prothoracic spiracle (acoustic spiracle) and through the acoustic trachea to reach the inside of the TMs in the forelegs (Fig. 1 *A*–*C*). Here, the acoustic trachea fulfills the role of an EC and will therefore be called EC from here on. The EC has considerable variation in morphology across the circa 7,000 living species of katydids (13), and this research focuses on a common type, which involves a large acoustic spiracle and a canal that gradually tapers as it approaches the tympanal organ (Fig. 1*C*) (14–20).

The symmetrical arrangement of the outer ear in katydids is not enough to enable the localization of sound—the insects are usually too small for their ears to detect interaural differences in time and amplitude for the relevant sounds in nature (6). Nevertheless, katydids overcome this problem as follows: 1) their ears are located in foreleg regions, with tracheal air spaces and chordotonal organs acting as sensitive proprioceptors to mechanical displacement (21). This arrangement produces more spatial separation than if they were positioned on the head, thorax, or abdomen. 2) The dual acoustic inputs form a pressure difference receiver at the TMs, caused by the convergence of the internal and external sound inputs.

As a pressure difference receiver, we define a system that creates a gradient in sound pressure across a membrane. In katydids, this is formed by the two sound inputs (external and internal) to the TMs (7) and via the fact that the sound wave coming through the internal part, the EC, is both amplified and slowed down compared with the external input (14, 15).

Significance

The katydid tympanal ears have outer, middle, and inner ear components analogous to mammalian ears. Unlike mammals, each ear has two tympana exposed to sound both externally and internally, with a delayed internal version arriving via the gas-filled ear canal (EC). The two combined inputs in each ear play a significant role in directional hearing. Here, we demonstrate that the major factor causing the internal delay is the EC geometry. The EC bifurcates asymmetrically, producing two additional internal paths that impose different sound velocities for each tympanum. Therefore, various versions of the same signal reach the ears at various times, increasing the chance to pinpoint the sound source. Findings could inspire algorithms for accurate acoustic triangulation in detection sensors.

Author contributions: C.D.S. and F.M.-Z. designed research; D.V., E.C., and F.M.-Z. performed research; E.C., T.J., and F.M.-Z. contributed new reagents/analytic tools; D.V., C.P., and C.W. collected data; D.V., E.C., S.A., C.P., C.D.S., T.J., C.W., and F.M.-Z. analyzed data; and D.V., E.C., and F.M.-Z. wrote the paper.

This article is a PNAS Direct Submission.

[1]D.V. and E.C. contributed equally to this work.

[2]To whom correspondence may be addressed. Email: ECeliker@lincoln.ac.uk or fmontealegrez@lincoln.ac.uk.

This article contains supporting information online at https://www.pnas.org/lookup/suppl/doi:10.1073/pnas.2017281118/-/DCSupplemental.

Published March 3, 2021.

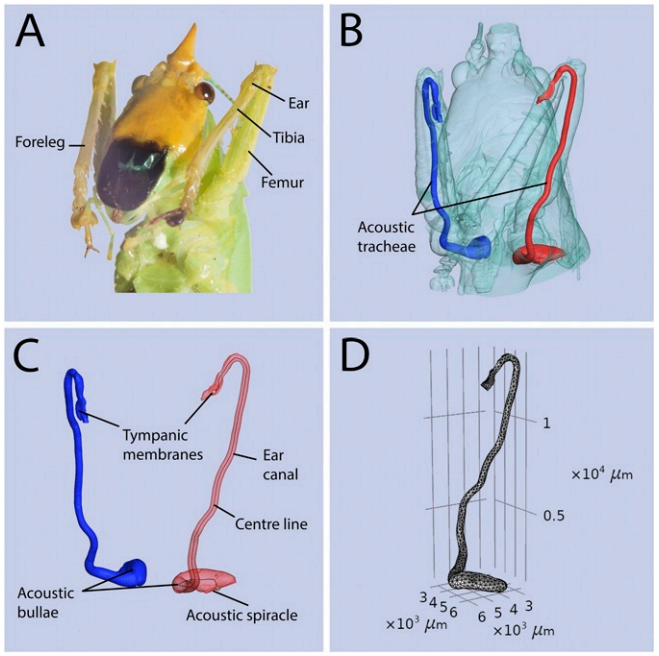

Fig. 1. Anatomy and 3D reconstruction of the katydid EC. (*A*) An image of the katydid *C. gorgonensis*. (*B*) The μ-CT image of the katydid highlighting the acoustic tracheae. (*C*) The components of the acoustic trachea. (*D*) The finite element mesh formed in the tracheal tube.

The reduction in sound velocity was first reported and inferred in Michelsen et al. (16) for crickets and Larsen (22) for crickets and katydids. This was later experimentally quantified (15). However, the underlying assumptions of the interpretation of results, such as the effect of the respiratory gases in the EC and propagation of sound in highly narrowing tubes being the cause of reduction of sound velocity (15, 23), have not been analyzed using experimental and numerical approaches.

Here, we experimentally determine the velocity of sound propagation inside the EC of the katydid *Copiphora gorgonensis* (Tettigoniidae, Copiphorini) and test the hypothesis that the gradually narrowing EC is the primary cause of any observed changes in sound velocity. Furthermore, to corroborate results, we investigate sound propagation velocity when the EC is filled with different gases, under the expectation that sound velocity will decrease in a narrow tube independently of the gas. Adding to the experimental results, we applied finite element analysis to simulate the propagation of sound in the precise geometry of all experimental ECs (Fig. 1*C*), obtained through microcomputed tomography (μ-CT). Both the experimental and numerical results demonstrate that EC geometry is the primary cause of sound velocity reduction within the katydid middle ear.

Results

We investigated factors leading to the reduction of sound velocity in the EC of *C. gorgonensis* in comparison with sound velocity in free air conditions (15), both experimentally and numerically. In particular, we considered the effect of the gas composition within both the left and right ECs of the specimen on the velocity reduction in three different categories: live insects, dead insects, and numerical models. The results from live and dead specimens were considered separately in order to observe the effect of the metabolic CO_2 reduction in the EC, which ensues after the specimen is dead. For each insect status, in addition to the gas composition inside the EC, we also analyzed whether the reduction of sound propagation velocity was affected by the length of the EC and the location of recording on the ATM or PTM. The EC bifurcates near the TMs, so that ATM and PTM lie on two separate branches: the anterior and posterior branches, respectively. The cross-sectional area of the anterior branch is smaller than that of the posterior branch by 2.28% in males and 5.67% in females (*SI Appendix*, Table S3); hence, the branches are asymmetrical.

We calculated the velocity of sound propagation through the EC by dividing the length of the EC with the time taken for a sound signal to transmit through it to the TM. To measure the time of sound transmission, the insect was mounted on a special platform that separates the internal and external sound inputs (Fig. 2). Sound was produced externally and passed into a probe loudspeaker, which delivered the signal into the EC, while the TMs were monitored with a microscanning laser Doppler vibrometer (LDV). The gas composition of the EC was manipulated by dispensing carbon dioxide gas (CO_2) into the acoustic spiracle via a microcapillary needle (*Materials and Methods*; *SI Appendix*, section 1 has details). CO_2 was used because the EC is derived from the respiratory system, and therefore, the gas could be present in naturally high concentrations; it is also known that sounds travel slower in CO_2 (*SI Appendix*, section 2 has details). Experiments were also carried out with air-filled EC. For these experiments, the natural gas composition of the specimen was flushed out, and it was left to refill by itself, so that by air, we refer to the gas composition inside the room (*SI Appendix*, section 3 has details). When compared with free-field sound velocity in air, sound velocity within the EC across live, dead, and numerically modeled data was significantly slower [F (2,45.16) = 68.19, $P < 0.001$] (Fig. 3 and Table 1). Both live and dead insects did not differ in their velocity reduction of 17.05% (live vs. dead: t ratio = 1.88, $P = 0.158$), but numerical data predicted a significantly greater velocity reduction than was found in live or dead insects, in air (vs. live: t ratio = 10.76, $P < 0.001$; vs. dead: t ratio = 9.09, $P < 0.001$) (Fig. 3*A* and Table 1). EC length did not affect the sound velocity reduction [F (1,8.13) = 1.60, P = 0.241], but the reduction of velocity was greater at the ATM [F (1,41.25) = 4.14, $P = 0.048$]. In live insects, with the EC filled with air, sound propagated to the ATM and PTM at mean velocities of 284 and 296 m/s, respectively. A numerical investigation on one specimen model showed sound propagation velocities of 224.84 and 228.59 m/s at the ATM and PTM, respectively, of the air-filled left EC; similar results were also obtained in the right EC (Fig. 4*B*).

Sound velocity data obtained at the TMs after the incident wave traveled through the CO_2-filled EC were significantly slower for all three insect statuses in comparison with free-field CO_2 sound velocity, but there was no significant difference among the different statuses [F (1,37.854) = 0.37, $P = 0.696$] (Fig. 3*B* and Table 1). More precisely, sound velocity of dead and live insects was 31.56% slower than free-field CO_2 sound velocity. Neither EC length [F (1,6.43) = 2.61, $P = 0.154$] nor sound velocity, at either tympanum, were significantly related to sound velocity with CO_2 present [F (1,36.41) = 0.54, $P = 0.467$].

To explore the effect of the EC radius on the sound propagation velocity inside of the ear in more detail, we also carried out numerical simulations after manipulating the EC geometry by changing its radius. Considering the tube to be filled with air or CO_2, we obtained the sound velocity from ECs with median radii 75 to 600 μm. The results are presented in Fig. 4*A*, from which it is evident that, regardless of the gas composition inside the tube, the ECs with a smaller radius display a greater reduction in sound velocity. In a separate simulation, we have also explored the effect of the asymmetric bifurcation of the EC on sound velocity. The results are presented in Fig. 4*B* and complement the results in Fig. 4*A* since sound is distributed asymmetrically, with higher velocity at the tympanum associated with the posterior branch of the EC, which is the wider branch.

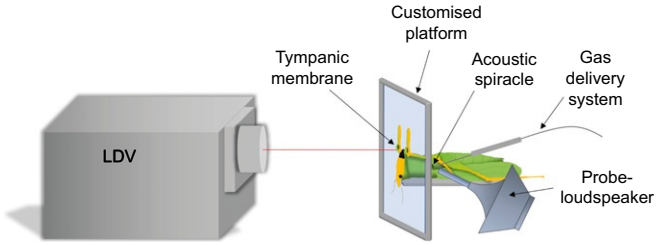

Fig. 2. Experimental preparation. The illustration shows the platform used to acoustically separate the ears from the spiracle, along with the gas replacement dispenser, acoustic stimulation, and laser recording system.

Discussion

Review of Findings. Our results demonstrate that sound propagation velocity was always reduced in relation to the expected free-field propagation velocity under normal conditions (Table 1), independent of gas composition in the EC. This suggests that the very narrow EC is the major factor that contributes to the observed reduction in velocity. This is further verified from the numerical results presented in Fig. 4*A*, which demonstrate a decreasing sound propagation velocity in the narrower ECs. This is consistent with the narrow tube theory developed in Benade (24) and Tijdeman (25). The narrow section of the EC, starting in the femur and ending in the base of the tibia (Fig. 1), has a relatively uniform radius of approximately 150 μm (Fig. 5), small enough to affect sound propagation velocity. Bifurcation of the EC at the tympanal level produces two shorter and narrower tube segments that reduce sound velocity further.

Ears like that of *C. gorgonensis* are believed to have at least two acoustic inputs. For *C. gorgonensis*, amplitude differences of around 15 dB are produced between the internal and external surfaces of the TMs (15). Our results show an internal time delay in live and dead insects (Table 1), supporting the findings in Jonsson et al. (15). The katydid ear has precise directionality for conspecific calls but omnidirectionality for predator detection (9). In the former, triangulation of the sound source is effective and accurate (e.g., 5° acuity) (26) but requires a locomotion behavior to overcome the frontal zone of ambiguity (27–29).

These insects determine the direction of the sound source through auditory differences in their independent ears (23); the differences, however, are caused by the interaction of an acoustic signal with its internally amplified and delayed counterpart at the TM as opposite to the externally arriving low amplitude and faster stimulus. Given that the signal delay in this system is further enhanced by the structure of the EC, we propose that this mechanism is included in the definition of the pressure difference receiver ears. Therefore, we redefine these ears as pressure–time difference receivers. A consequence of the EC geometry-mediated time delay is the possible distortion (compression/rarefaction) of the longitudinal waves as they enter the narrow part of the EC shortly after arriving at the spiracle, due to the velocity difference. This could lead to continual waveform interference and intermodulation of the waves as they move down the EC, which could potentially act as a delay-line filter for certain frequencies, and thus, deserves further investigation.

Through additional investigation, it has been observed that the gas composition contributes to the rate of velocity reduction. The numerical results show that sound propagation slows down 32.47% in air and 28.19% in CO_2, when compared with its respective free-field velocities under normal conditions (Table 1). These results imply that the rate of reduction in air is 4.3% less compared with that in CO_2. We believe that these discrepancies are associated with the physical properties of each gas, and to corroborate this, we ran numerical simulations where the EC was filled with helium (He). This also projected a reduction in sound velocity (*SI Appendix*, section 4 and Table S1).

As a further demonstration that different gases will interact with EC geometry in different ways, we also consider the theoretical solution developed by Benade (24) for the phase velocity in a narrow tube. This is defined by

$$v = c \cdot \left(1 - \frac{1}{r_v\sqrt{2}} - \frac{\gamma - 1}{r_t\sqrt{2}}\right), \qquad [1]$$

where c is the speed of sound in open space; γ is the ratio of specific heats; and r_v, r_t are variables proportional to the ratio of the tube radius to the viscous and thermal boundary-layer thicknesses, respectively, and are strongly dependent on gas density. We have assumed the propagation velocity for three different gases (air, He, and CO_2), taking the tube radius to be equal to the median EC radius of 150 μm and the sound stimulus to be at 23 kHz (the variables used for calculating the phase velocity have been outlined in *SI Appendix*, Table S1).

The results (*SI Appendix*, Table S1) show that in air there is a reduction of 7.3% from free-field propagation. In CO_2, this reduction was around 4.5%, whereas for He, it was 24.7%. There is an expected difference in the numerical results obtained in the EC and with the use of formula (**1**) since the tube for which formula (**1**) holds has a uniform radius and is assumed to have a rigid wall.

Formula (**1**) demonstrates that the reduction of sound velocity in tubes is also affected by the thickness of the viscous and thermal boundary layers formed near the tube wall, which in turn, depend on the tube radius and the gas properties. Based on the theoretical results, it can be concluded that differing rates of velocity reduction obtained in the EC for different gas compositions result from the viscous and thermal boundary layers formed near the EC wall, whose effects are stronger in narrower tubes.

When the experimental results are compared with the numerical model in CO_2, there is a consistent reduction in velocity, in air; however, the numerical model predicts a greater decrease in sound velocity than what we observed experimentally. Furthermore, the reduction rate obtained in air (16.24% in live insects and 17.60% in dead insects) is not as large as the results obtained in Jonsson et al. (15), where velocity reduction was 25%. This is attributable to our study utilizing precise and consistent μ-CT measurements to determine the tracheal length, whereas the previous study (15) used multiple approaches. The higher variation

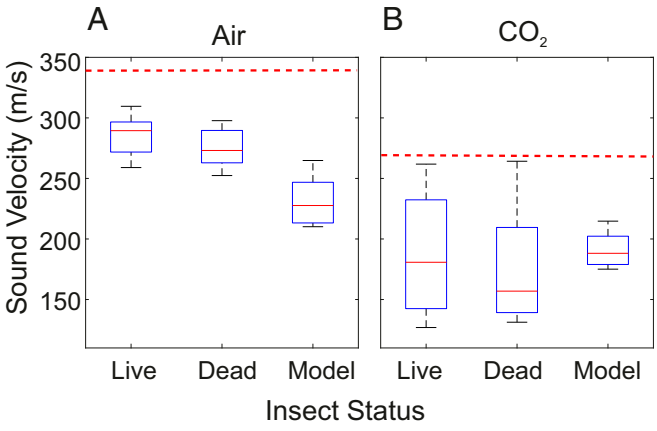

Fig. 3. Sound propagation velocity measured experimentally and numerically. Experimental procedures were conducted in live and dead specimens. (*A*) EC filled with air. The dashed line represents the free-field sound velocity in air: 343 m/s. (*B*) EC filled with CO_2. The dashed line represents the free-field sound velocity in CO_2: 267 m/s.

Table 1. A summary of data across all treatments

	Free field	Live	Dead	Numerical
Air				
Sample size	NA	$n_S = 8$, $n_{EC} = 14$	$n_S = 8$, $n_{EC} = 15$	$n_S = 7$, $n_{EC} = 13$
Mean sound velocity (m/s) ± SD	343	289.109 ± 16.245	280.172 ± 17.606	231.638 ± 16.763
% reduction from free-field sound velocity	NA	15.712	18.317	32.467
Mean EC length (mm) ± SD	NA	17.126 ± 0.998	17.067 ± 0.938	17.314 ± 0.935
Mean travel time (ms) ± SD	NA	0.0595 ± 0.00545	0.0611 ± 0.00445	0.0750 ± 0.00485
CO_2				
Sample size	NA	$n_S = 8$, $n_{EC} = 14$	$n_S = 8$, $n_{EC} = 14$	$n_S = 7$, $n_{EC} = 13$
Mean sound velocity (m/s) ± SD	267	184.318 ± 42.546	181.13 ± 41.857	191.728 ± 12.046
% reduction from free-field sound velocity	NA	30.968	32.161	28.192
Mean EC length (mm) ± SD	NA	17.126 ± 0.998	17.095 ± 0.968	17.314 ± 0.935
Mean travel time (ms) ± SD	NA	0.0972 ± 0.00205	0.0987 ± 0.00209	0.0905 ± 0.00524

Sample size shows both the number of specimens (n_S) and number of ECs (n_{EC}). NA, not applicable.

displayed in the sound velocity measurements in CO_2 likely results from random error in gas dispensation.

Differences between the experimental and numerical results can also be attributed to some simplifying assumptions applied in the model. For instance, we assumed that the lumen of the EC is smooth. Instead, the EC is derived from the respiratory trachea built up of taenidia, which generally take the form of spiral thickenings of the tracheal walls joined by soft material, forming an irregular sinuous surface. In the model, the gas is also assumed to be quiescent; hence, it is at rest as the sound stimulus enters the trachea, which in reality, it is not since the tracheal tube is part of the respiratory system of the insect.

As follows from Table 1, the largest discrepancies between the experimental and numerical results are present in the data related to the sound velocity from the air-filled ECs, which suggests some differences of the gas compositions inside the ECs during the experiments and the numerical simulations. The gas content inside the ECs for the experiments with air was ambient atmospheric gas composition; hence, the EC might not be completely free of CO_2. However, for the numerical simulations the air filling the ECs is assumed to be under standard conditions and thus, does not contain any excess CO_2. Nonetheless, both the experimental and numerical results show that even though the gas composition inside the EC plays a part in the rate of velocity reduction inside the tube, the key component causing it is the complex EC geometry.

The Use of CO_2 as a Potential Mechanism to Hone Sound Localization. The purpose of filling the EC with CO_2 was purely for testing the mechanics of the EC, as the EC containing pure CO_2 is an unrealistic situation in nature. However, since the results of these mechanical experiments show that CO_2 causes the sound to propagate even slower than the normal (already reduced) sound velocity in the EC, we would like to discuss a potential effect of metabolic CO_2 on binaural hearing.

In insects where the respiratory trachea are associated with active muscular-controlled spiracle openings, concentration of CO_2 could be significantly higher when those spiracles are closed. When the spiracles are subsequently opened, the levels of CO_2 and O_2 equilibrate with those of air (17). During those open and closed phases, sound propagation velocity would be affected, due to the varying CO_2 concentration inside the EC. The degree of concentration change and the effect on propagation velocity are unknown, but we believe this idea should be further investigated, especially in species that have control of spiracle valves and exhibit tracheal and acoustic connections between the left and the right ECs, like field crickets. To the best of our knowledge, the effect of opened or closed EC spiracles on sound propagation velocity and sound reception at the level of the tympana and the crista acustica has never been investigated [Michelsen et al. (16) and Larsen et al. (22)].

Dual-Input Ears in the Animal Kingdom. Other animals, including some insects and tetrapods, utilize pressure difference receivers to localize sound. These include grasshoppers (30), lizards (31), crocodilians (32), and birds. Unlike in katydids, the pressure difference in these animals occurs between the membranes of two internally coupled ears. A signal transmitting internally from one TM to another may suffer attenuation or depending on the interaural distance and frequency of the signal, a time delay. This mechanism can present problems for smaller organisms such as the grasshopper (Acrididae). Grasshopper ears are located at lateral surfaces of the almost cylindrical body, on the first abdominal segment. The tympana are connected by a series of sound-guiding air sacs (30), permitting sound to internally travel from one TM to the other. The vibration of the TMs, measured using LDV recordings, shows the occurrence of nulls (i.e., frequencies where eardrum vibration is canceled because its two surfaces receive sounds with an identical amplitude and phase) (23).

The katydid outer ear reported here shows similarities with some bird ears. Avian ears are located at the side of the head, and evidence suggests that some species utilize pressure difference receivers to localize sound (33–35). Across taxa, the documented anatomy of the avian EC varies from the basic interaural canal of the barn owl (*Tyto alba*) (36) to the complex network of tubes described in the zebra finch (*Taeniopygia guttata*) (37). The zebra finch overcomes the size limitations of sound localization through a delayed interaural signal (35). The mechanism behind this delay is unknown but could result from a series of narrow tubes that internally connect each ear (37). The TMs of the zebra finch are directly connected by an interaural canal but are also interconnected by several narrow canals [the figure in Larsen et al. (37)]. Perhaps the most significant of the narrow pathways are the superolatero-orbital canals. These begin above the interaural canal, at the sides of the head, arching upward to join together in a sinus on the forehead (superoantero-orbital sinus). The end result is a 27-mm-long canal with a cross-sectional area of 400 μm^2 (radius = 11.3 μm). The superoantero-orbital sinus also associates with other narrow canals, both of which run down the longitudinal plane of the head. Resembling an exponential horn, the 5-mm-long hypomedial-orbital tube connects the sinus to the interaural canal. Near the sinus, at its most narrow point, the cross-sectional area is 400 μm^2. The narrowest tube is 7-mm long and has a cross-sectional area of 100 μm^2 (radius = 5.6 μm). This extends from the sinus to a medium-sized tube that runs parallel to the interaural canal. Proposed to be air filled (37), these narrow tubes resemble the geometry of the

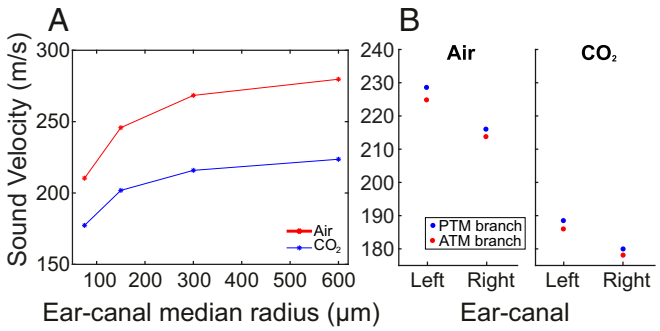

Fig. 4. Finite element analysis of the effect of the EC radius and asymmetric EC bifurcation on sound speed. (*A*) The speed of sound measured at the end of the ECs with different radii, while filled with air or CO_2, using finite element analysis. (*B*) The numerical results of the sound velocity as it reaches the ATM and the PTM from the anterior and posterior branches, respectively, of a specimen through air-filled left and right ECs and CO_2-filled left and right ECs of a specimen. The velocity differences between left and right ECs are due to small variations in the μ-CT measurements of the ECs.

katydid EC. If sound does indeed reach these canals, then our models display the potential effect they could have on signal transmission through the internal pathways in birds, and any role in sound localization and potential signal delay warrants investigation.

Another relevant aspect of narrowing tubes and the reduction in sound velocity in katydids (Fig. 4*A*) is the potential effect of the EC division at the position of the tympanal organ (Fig. 6). The EC divides into two branches prior to reaching the inner ear: an anterior branch leads to the ATM, and a posterior branch leads to the PTM (Fig. 4*B*). The anterior branch is narrower in width than the posterior branch and is also adjacent to the auditory sensilla (38). Our experimental results show an asymmetrical response of the TMs to sound conduction from the EC, as the sound first arrives to the PTM and then to the ATM. These results are also supported by our numerical simulations in the precise geometry of the EC and the EC branches (Fig. 4*B*). The sound arrives first at the PTM through the posterior branch, which is wider than the anterior branch (*SI Appendix*, Table S3). This parallels the results presented in Fig. 4*A*, which demonstrate that the EC radius and sound velocity have a directly proportional correlation (Fig. 6 *C* and *D*).

The experimental data from live insects, when the EC is filled with air, showed on average a sound propagation velocity difference of 12 m/s as the sound wave hits the TMs due to a difference in arrival time of 4.95 μs between ATM and PTM. This is equivalent to a phase shift of 40.98° at 23 kHz. The actual effects of the delay on the crista acustica traveling wave are not known. However, calculating the theoretical gain for two superpositioned waves of equal frequency, equal amplitude A and the aforementioned phase shift gives the amplitude sum as 1.75A (without the phase shift, this would equal 2A), which could theoretically be a significant amplitude reduction at, for example, the level of the acoustic vesicle, caused by the temporal delay of the arriving signal at the TMs. The numerical results showed a smaller difference of 3.75 m/s (Fig. 4*B*) in propagation speed, which can be attributed to the small changes in the bifurcation morphology during reconstruction, the flat surface of the EC that contrasts with the irregular surface. Nevertheless, the numerical results are in analogy to the experimental data and demonstrate that the sound arrives at the PTM first before reaching the ATM after a small time delay.

The asymmetrical response of the TMs could also affect the mechanical interaction of the sound waves acting on the external surface of both TMs by, for example, destructive interference, as the flaps or pinna covering the TMs produce an asymmetrical sound pressure effect around the ear (9): the two TMs work in concert as a type 1 cantilever, magnifying the input force to provide a greater output force (39). The ear flaps in *C. gorgonensis* and many other katydids (e.g., Conocephalinae and Pseudophyllinae) seem to enhance a highly directional response of both TMs (9, 40), and if sound energy entering a spiracle is weak [depending on the position of the sound source (41)], it can potentially lead to an asymmetric destructive interference between internal and external inputs, in a single ear. When taking into account the two external inputs at each TM, a single ear may face a total of four acoustic inputs (compared with only one for the human ear). Therefore, even though the spiracle and the EC system have traditionally been appreciated as the nondirectional component of the auditory receiver (9), our results suggest that the role played by the asymmetrical conduction from the TMs in directional hearing warrants further investigation. Do the bifurcations at the tympanal cavities predominantly contain CO_2? If true, how are the mechanics of the TMs when they are externally exposed to ambient air while internally exposed to concentrated CO_2?

Materials and Methods

Experimental Design. This research combines experimental and numerical approaches to infer the cause of sound velocity reduction inside the acoustic trachea of katydids. The experimental aspect involves measuring the time for an acoustic signal to transmit through the EC of a katydid and determining the length of the EC. This enables sound velocity to be calculated by dividing the length of the EC by the time it takes the sound stimulus to reach the TM. To achieve this, a special platform that isolates the external and internal auditory inputs is utilized (5, 15), along with an array of probe loudspeakers, microphones, function generators, and an LDV. We record the effect of different gas compositions on the sound propagation velocity. Gas is added to the EC through the use of a customized delivery system (*SI Appendix*, section 1 has more details).

Experimental Animals. This study used specimens of *C. gorgonensis* that were eighth-generation descendants of a colony collected in November 2015 from the National Natural Park Gorgona, Colombia (latitude 2°58′7.4208″N; longitude 78°11′10.4964″W). Insects were maintained in communal vivaria (temperature 22 °C to 27 °C). A total of nine adult individuals (five males and four females) were used in this study (n = 17 ears).

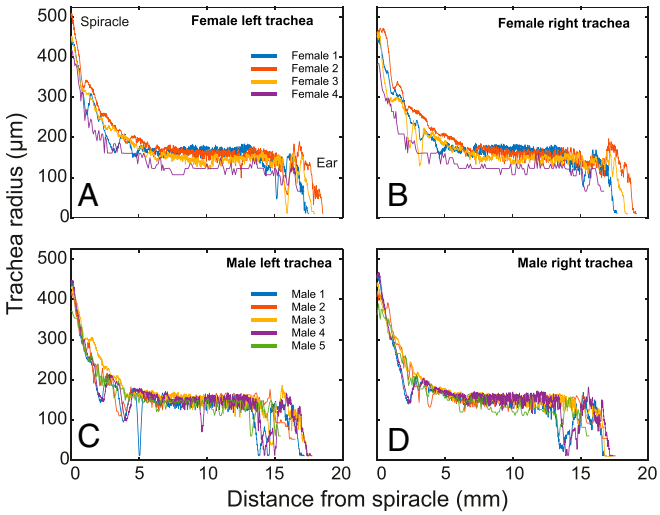

Fig. 5. Quantitative relationship between EC (trachea) radius and length. Measured distance displayed from the acoustic spiracle to the tympanal organ area in males and females of *C. gorgonensis*. (*A*) Female left EC. (*B*) Female right EC. (*C*) Male left EC. (*D*) Male right EC.

Experimental Setup. To observe the effects of the internal pathway only, we isolated the internal and external sound inputs. We did this by mounting the insect on a customized platform (Fig. 2). The platform consists of two Perspex panels that fit together, the dorsal of which encompasses a central notch for the insect's head along with two adjacent holes for the forelegs. These panels are held together within a metal frame [additional details are in the work by Montealegre-Z et al. (5) and *SI Appendix*, section 5].

A 23-kHz pure tone is produced by a function generator (SDG1000 Series Function/Arbitrary Waveform Generator; Siglent Technologies Co. Ltd.) and emitted via an MF1-S 1 Multi Field Speaker (Tucker Davis Technologies) with a modified probe attachment (*SI Appendix*, section 6 and Fig. S1).

Prior to each experiment, a standardized reference point was recorded. The probe loudspeaker was mounted onto a micromanipulator (World Precision Instruments, Inc.). A calibrated 1/8-inch (3.2-mm) microphone (Brüel & Kjær) was held in a clamp, and the loudspeaker probe was positioned 2 mm away from the microphone's protective cap. The time taken for sound to travel from the loudspeaker probe to the microphone was recorded as the reference time.

The mounted insect was positioned in front of the LDV, and the laser point focused on a TM (Figs. 1 and 2). A gas delivery system (enabling the manipulation of the gas composition between experiments) was introduced behind the prothoracic side keel, directed toward the acoustic spiracle (Fig. 1 and *SI Appendix*, section 1). The probe loudspeaker was then placed 2 mm away from the spiracle (matching the distance of the microphone reference signal), allowing sound to travel through the acoustic trachea and vibrate the tympanum (Fig. 1). For each ear, the LDV was used to record the time for the signal vibrations to arrive at the tympanum, measured as tympanal displacement.

Recordings were first taken without changes to the gas composition within the EC (normal conditions). The time taken for sound to travel from the loudspeaker to the TM was noted and used as a benchmark throughout the experiment, to indicate when the gas composition in the EC was normal. Then, over a period of 5 s, pure CO_2 (Genuine Innovations) was introduced to the canal via the gas delivery system, and the time was recorded again (*SI Appendix*, section 1). The CO_2 was left to diffuse out of the trachea until the signal reaching the tympanum returned to normal. This was replicated three times, before being repeated on the opposite foreleg. Experiments were conducted at ambient temperatures of 19.8 °C and 25.0 °C, with the body temperatures of the insects ranging from 23.6 °C to 28.1 °C.

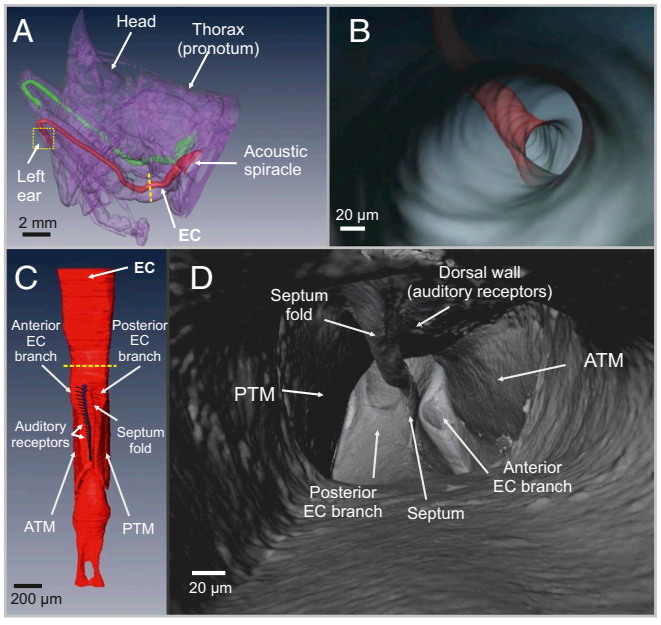

Fig. 6. External and internal morphology of the EC showing the tracheal division at the tympanal organ location. (*A*) Lateral view of the body in transparency showing left and right ECs. (*B*) Internal view inside the EC. (*C*) Close-up view of the ear section extracted from the dashed box in *A*. (*D*) Internal view inside the EC showing the branch division of the trachea at the tympanal organ location. Camera was placed inside the EC lumen approximately at the location of the yellow dashed line in *C*.

Anatomical Measurements of the EC. The anatomy of the EC was examined using X-ray μ-CT and three-dimensional (3D) reconstruction, using standard biomedical imaging software following the published protocols (15). All of the specimens were scanned with a Bruker SkyScan 1272 (Bruker Micro-CT) at 50 kV and 200 mA, with a voxel size ranging from 3.12 to 10.99 μm. Reconstruction and automated measurements of EC were carried out with AMIRA (version 6.7; VSG). The EC lengths of all individuals were measured from the 3D reconstructions using the Center Line Tree module in AMIRA.

Sound Analysis and Calculation of Velocity. The first local minimum of the sine wave chirp was used to obtain time measurements (*SI Appendix*, section 7 has more details on the reference signal). The time delay between the reference signal and the amplitude signal of the tympanum was obtained using MatLab (R2014a; The Math-Works, Inc.). This delay was used to calculate the velocity of sound propagation through each EC—dividing the EC lengths obtained from 3D segmentations by the respective mean time delay.

Mathematical Model and Numerical Simulations. The numerical results are based on the following system of equations.

Let Ω denote the EC of *C. gorgonensis*, which is the domain of our mathematical model formed by the union of two parts: Ω_f is the inside of the EC (the fluid domain) and Ω_s is the EC wall (solid domain), which intersect at the interface $\gamma = \Omega_s \cap \Omega_f$. The boundary of Ω consists of γ_1, which denotes the acoustic spiracle; γ_2, which denotes the TM; and γ_3, which denotes the outer surface of the wall.

In the fluid domain Ω_f, the propagation of the sound wave is modeled with the use of the scalar wave equation, which also takes into account the viscosity of the quiescent fluid. This is represented with the following equation and initial conditions:

$$\frac{\partial^2 p}{\partial t^2} + \frac{1}{\rho_f}\left(\frac{4}{3}\mu + \mu_B\right)\frac{\partial \nabla p}{\partial t} = c^2 \Delta p \text{ in } \Omega_f \times (0, T], \quad [2]$$

$$p(\mathbf{x}, 0) = 0, \ \frac{\partial p}{\partial t}(\mathbf{x}, 0) = 0 \text{ in } \Omega_f, \quad [3]$$

where $T > 0$ is a fixed positive time, c = speed of sound, μ = dynamic viscosity, μ_B = bulk viscosity, ρ_f = fluid density, $\nabla = (\frac{\partial}{\partial x}, \frac{\partial}{\partial y}, \frac{\partial}{\partial z})$, and $\Delta = \nabla^2$. The dependent variable $p = p(\mathbf{x}, t)$ is the time-dependent sound pressure at the spatial point $\mathbf{x} = (x, y, z)$.

A harmonic incident wave enters into the EC through the spiracle with a frequency of 23 kHz and an amplitude of 1 Pa, traveling at 343 m/s, represented by the boundary condition

$$\mathbf{n} \cdot \left(\frac{1}{\rho_f}\nabla p\right) + \frac{1}{\rho_f}\left(\frac{1}{c}\frac{\partial p}{\partial t}\right) = \mathbf{n} \cdot \left(\frac{1}{\rho_f}\nabla p_i\right) + \frac{1}{\rho_f}\left(\frac{1}{c}\frac{\partial p_i}{\partial t}\right) \quad [4]$$

on γ_1, where

$$p_i = \sin\left(2\pi \times 23000\left(t - \frac{(\mathbf{x} - \mathbf{e}_k)}{c|\mathbf{e}_k|}\right)\right),$$

and $\mathbf{e}_k$ is the wave direction.

Taking into account the impedance of the TM, we request the boundary condition (**5**) given below is satisfied on γ_2:

$$\mathbf{n} \cdot \frac{1}{\rho_f}\nabla p = \frac{1}{Z_i}\frac{\partial p}{\partial t}, \quad [5]$$

where Z_i is the magnitude of the specific acoustic impedance of the TM.

Next, we consider the displacement in the elastic wall due to the sound propagating inside the EC. This is represented by the elastic wave Eq. **6** given below, which models the mechanical waves in the structure Ω_s assuming small deformations (42). We make the simplifying assumption that the EC wall is built of an isotropic, incompressible, and homogeneous material. Eq. **6** also accounts for the damping properties of the EC wall:

$$\rho_s \frac{\partial^2 \mathbf{u}_s}{\partial t^2} + \rho_s \alpha_{dM} \frac{\partial \mathbf{u}_s}{\partial t} = \nabla \cdot \left(\sigma(\mathbf{u}_s) + \beta_{dK}\frac{\partial \sigma}{\partial t}\right) \text{ in } \Omega_s \times (0, T], \quad [6]$$

$$\mathbf{u}_s(\mathbf{x}, 0) = \mathbf{0}, \ \frac{\partial \mathbf{u}_s}{\partial t}(\mathbf{x}, 0) = \mathbf{0} \text{ in } \Omega_s, \quad [7]$$

where ρ_s is the density of the wall and the components of the stress tensor $\sigma(\mathbf{u}_s)$ are

$$\sigma_{ij} = \frac{E}{1+\nu}\epsilon_{ij} + \frac{E\nu}{(1+\nu)(1-2\nu)}\delta_{ij}\sum_{k=1}^{3}\epsilon_{kk},\ i,j=1,2,3, \quad [8]$$

with E = Young's modulus; ν = Poisson's ratio; $\epsilon_{ij} = \frac{1}{2}\left(\frac{\partial \mathbf{u}_{si}}{\partial x_j} + \frac{\partial \mathbf{u}_{sj}}{\partial x_i}\right)$ is the strain tensor; δ_{ij} is the Kronecker-delta function; and the dependent variable $\mathbf{u}_s$ is the displacement vector in Ω_s. Furthermore, the Rayleigh damping parameters α_{dM} and β_{dK} satisfy the following relation between the damping ratio ξ_i and the natural frequencies ω_i of an undamped system:

$$\xi_i = \frac{\alpha_{dM}}{2\omega_i} + \frac{\omega_i\beta_{dK}}{2}, \quad [9]$$

where α_{dM} and β_{dK} are the mass proportional and stiffness proportional Rayleigh damping coefficients, respectively.

On γ_3, we specify the boundary condition as

$$\sigma_{ij}\cdot n_j = 0,\ i,j=1,2,3, \quad [10]$$

so that there is no external stress on the wall.

Finally, at the interface γ, the defined fluid and solid systems are coupled. The coupling includes the fluid load on the structure and the structural acceleration as experienced by the fluid:

$$\mathbf{n}\cdot\frac{1}{\rho_f}\nabla p = -\mathbf{n}\cdot(\mathbf{u}_s)_{tt}, \quad [11]$$

$$F_A = p\mathbf{n}, \quad [12]$$

where $\mathbf{n}$ is the surface normal and F_A is the force per unit area experienced by the structure.

As well as the pressure distribution in the EC for the time interval $(0, T]$, by solving system (**2**–**12**), we are also able to obtain the time taken for the sound stimulus to reach the TM. Using this, we calculate the speed of sound during transmission by the elementary formula

$$speed = \frac{distance}{time},$$

where *distance*= length of the EC.

For spatial discretization, the numerical solution of the variational form of the introduced equations, along with the defined boundary conditions, is obtained with the finite element method using the commercial software Comsol Multiphysics version 5.5 (43).

The finite element mesh constructed in the EC is demonstrated in Fig. 1. The tetrahedral elements forming the mesh in Ω_f have the restriction that the diameter of each element is less than the quantity

$$\frac{\text{wavelength of sound wave}}{30}.$$

The mesh in Ω_f is connected to the mesh on Ω_s, which is formed using shell elements of Mixed Interpolation of Tensorial Components type (44), a common mesh type used for capturing various shell behaviors. The solution of the system of finite element equations in space is based on Quadratic Lagrange elements for all of the dependent variables.

For the discretization of the time derivatives in system (**2**–**12**), the Generalized Alpha Method is employed, with a time step of $\tau = 2.174\times10^{-8}$ s. Taking into account that the frequency of the sound stimulus is 23 kHz, we took $T = 5/(23\text{ kHz}) = 2.174$ s, so that we assumed the sound stimulus has five cycles at 23 kHz.

The outlined equations are solved using the 3D Transient Acoustic-Shell interaction module of Comsol Multiphysics (43) (*SI Appendix*, Table S2 shows the values of the parameters used in Eqs. **2**–**12**).

For the simulations that have been carried out on ECs with different radii, the conditions outlined above have been kept the same. The geometry of the EC model was changed by using the "scale" feature of Comsol Multiphysics version 5.5 (43).

Data Processing and Statistical Analysis. During each experiment, the time taken for sound to propagate through the EC to the TM was recorded using LDV. For each EC sample, the mean of a minimum of three replicates was calculated. Postexperiment, recordings were standardized against a reference recording. For some recordings using CO_2 gas, the reference signal was invalidated due to too much gas dispensation, and therefore, these recordings were removed from the analysis. The remaining values, along with length data obtained from μ-CT data, were then used to calculate the mean sound propagation velocity for each individual EC. The mean sound propagation velocity and SD were taken and listed in Table 1.

Sound velocity in acoustic trachea was analyzed using Gaussian linear mixed effects models. Velocity was the dependent variable, with tracheal length as a covariate and tympanum (ATM/PTM) and status (live, dead, numerical model) as fixed factors. To account for repeated measures of the same individual and EC, EC (right/left) was nested within individual as a random factor. Linear mixed effects models were run using lmerTest (45) in R 4.0.0 (45). Residuals from both models were checked for normality and heteroscedasticity and found to meet model assumptions. Post hoc testing was carried out using estimated marginal means from the emmeans package (46).

Data Availability. Numerical simulations, experimental data (laser Doppler vibrometry recordings), Comsol model files, and μ-CT stereolithography files (in .stl format) are available in Dryad (DOI: 10.5061/dryad.2547d7wnn; deposited 8 November 2020).

ACKNOWLEDGMENTS. This study is funded by European Research Council Grant ERCCoG-2017-773067 (to F.M.-Z. for the project "The Insect Cochlea"). T.J. is supported through the European Commission via Horizon 2020 Marie Skłodowska-Curie Fellowship 829208 (InWingSpeak).

1. S. A. Gelfand, *Hearing: An Introduction to Psychological and Physiological Acoustics* (CRC Press, 2005).
2. A. S. Tucker, Major evolutionary transitions and innovations: The tympanic middle ear. *Phil. Trans. R. Soc. B* **372**, 20150483 (2017).
3. R. E. Lombard, J. R. Bolt, Evolution of the tetrapod ear: An analysis and reinterpretation. *Biol. J. Linn. Soc. Lond.* **11**, 19–76 (1979).
4. H. E. Heffner, R. S. Heffner, The evolution of mammalian sound localization. *Acoust. Today* **12**, 20–35 (2016).
5. F. Montealegre-Z, T. Jonsson, K. A. Robson-Brown, M. Postles, D. Robert, Convergent evolution between insect and mammalian audition. *Science* **338**, 968–971 (2012).
6. M. Hartbauer, H. Römer, From microseconds to seconds and minutes—time computation in insect hearing. *Front. Physiol.* **5**, 138 (2014).
7. D. Robert, "Directional hearing in insects" in *Sound Source Localization*, A. N. Popper, R. R. Fay, Eds. (Springer Handbook of Auditory Research, Springer, New York, NY, 2005), vol. 25, pp. 6–35.
8. J. E. Yack, The structure and function of auditory chordotonal organs in insects. *Microsc. Res. Tech.* **63**, 315–337 (2004).
9. W. J. Bailey, R. O. Stephen, Directionality and auditory slit function: A theory of hearing in bushcrickets. *Science* **201**, 633–634 (1978).
10. K. Rajaraman, N. Mhatre, M. Jain, M. Postles, T. Balakrishnan, D. Robert, Low-pass filters and differential tympanal tuning in a paleotropical bushcricket with an unusually low frequency call. *J. Exp. Biol.* **216**, 777–787 (2012).
11. E. Hoffmann, M. Jatho, The acoustic trachea of Tettigoniids as an exponential horn: Theoretical calculations and bioacoustical measurements. *J. Acoust. Soc. Am.* **98**, 1845–1851 (1995).
12. J. Shen, A peripheral mechanism for auditory directionality in the bushcricket *Gampsocleis gratiosa*: Acoustic tracheal system. *J. Acoust. Soc. Am.* **94**, 1211–1217 (1993).
13. W. J. Bailey, "The ear of the bushcricket" in *The Tettigoniidae: Biology, Systematics and Evolution*, W. J. Bailey, D. C. F. Rentz, Eds. (Crawford House Press, Bathurst, Australia, 1990), pp. 217–247.
14. E. Celiker, T. Jonsson, F. Montealegre-Z, The auditory mechanics of the auter ear of the bush cricket: A numerical approach. *Biophys. J.* **118**, 464–475 (2020).
15. T. Jonsson, F. Montealegre-Z, C. D. Soulsbury, K. A. Robson Brown, D. Robert, Auditory mechanics in a bush-cricket: Direct evidence of dual sound inputs in the pressure difference receiver. *J. R. Soc. Interface* **13**, 20160560 (2016).
16. A. Michelsen, A. V. Popov, B. Lewis, Physics of directional hearing in the cricket *Gryllus bimaculatus*. *J. Comp. Physiol. A* **175**, 153–164 (1994).
17. M. J. Klowden, *Physiological Systems in Insects* (Elsevier, ed. 2, 2008).
18. K. N. Prestwich, T. J. Walker, Energetics of singing in crickets: Effect of temperature in three trilling species (Orthoptera: Gryllidae). *J. Comp. Physiol.* **143**, 199–212 (1981).
19. G. Wendler, G. Löhe, The role of the medial septum in the acoustic trachea of the cricket *Gryllus bimaculatus*. *J. Comp. Physiol. A* **173**, 557–564 (1993).
20. A. Michelsen, K. Rohrseitz, K. G. Heller, A. Stumpner, A new biophysical method to determine the gain of the acoustic trachea in bushcrickets. *J. Comp. Physiol. A* **175**, 145–151 (1994).
21. A. Stumpner, D. Von Helversen, Evolution and function of auditory systems in insects. *Naturwissenschaften* **88**, 159–170 (2001).
22. O. N. Larsen, Mechanical time resolution in some insect ears. *J. Comp. Physiol. A* **143**, 297–304 (1981).
23. A. Michelsen, O. N. Larsen, Pressure difference receiving ears. *Bioinspir. Biomim.* **3**, 011001 (2008).
24. A. H. Benade, On the propagation of sound waves in a cylindrical conduit. *J. Acoust. Soc. Am.* **44**, 616–623 (1968).

25. H. Tijdeman, On the propagation of sound waves in cylindrical tubes. *J. Sound Vib.* **39**, 1–33 (1975).
26. W. J. Bailey, The tettigoniid (Orthoptera: Tettigoniidae) ear: Multiple functions and structural diversity. *Int. J. Insect Morphol. Embryol.* **22**, 185–205 (1993).
27. W. J. Bailey, P. B. Yeoh, Female phonotaxis and frequency discrimination in the bushcricket *Requena verticalis*. *Physiol. Entomol.* **13**, 363–372 (1988).
28. E. Ofner, J. Rheinlaender, H. Römer, Spatial orientation in the bushcricket leptophyes punctatissima (phaneropterinae; Orthoptera). II. Phonotaxis to elevated sound sources on a walking compensator. *J. Comp. Physiol. A* **193**, 321–330 (2007).
29. H. Römer, Directional hearing in insects: Biophysical, physiological and ecological challenges. *J. Exp. Biol.* **223**, jeb203224 (2020).
30. A. Michelsen, K. Rohrseitz, Directional sound processing and interaural sound transmission in a small and a large grasshopper. *J. Exp. Biol.* **198**, 1817–1827 (1995).
31. J. Christensen-Dalsgaard, G. A. Manley, Directionality of the lizard ear. *J. Exp. Biol.* **208**, 1209–1217 (2005).
32. C. E. Carr, D. Soares, J. Smolders, J. Z. Simon, Detection of interaural time differences in the alligator. *J. Neurosci.* **29**, 7978–7990 (2009).
33. J. J. Rosowski, J. C. Saunders, Sound transmission through the avian interaural pathways. *J. Comp. Physiol. A* **136**, 1831190 (1980).
34. O. N. Larsen, R. J. Dooling, A. Michelsen, The role of pressure difference reception in the directional hearing of budgerigars (*Melopsittacus undulatus*). *J. Comp. Physiol. A* **192**, 1063–1072 (2006).
35. M. B. Calford, R. W. Piddington, Avian interaural canal enhances interaural delay. *J. Comp. Physiol. A* **162**, 503–510 (1988).
36. L. Kettler, J. Christensen-Dalsgaard, O. N. Larsen, H. Wagner, Low frequency eardrum directionality in the barn owl induced by sound transmission through the interaural canal. *Biol. Cybern.* **110**, 333–343 (2016).
37. O. N. Larsen, J. Christensen-Dalsgaard, K. K. Jensen, Role of intracranial cavities in avian directional hearing. *Biol. Cybern.* **110**, 319–331 (2016).
38. M. Bangert, K. Kalmring, T. Sickmann, R. Stephen, M. Jatho, R. Lakes-Harlan, Stimulus transmission in the auditory receptor organs of the foreleg of bushcrickets (Tettigoniidae). I. The role of the tympana. *Hear. Res.* **115**, 27–38 (1998).
39. F. Montealegre-z, D. Robert, Biomechanics of hearing in katydids. *J. Comp. Physiol. A* **201**, 5–18 (2015).
40. A. C. Mason, G. K. Morris, P. Wall, High ultrasonic hearing and tympanal slit function in rainforest katydids. *Naturwissenschaften* **78**, 365–367 (1991).
41. R. Lakes−Harlan, J. Scherberich, Position-dependent hearing in three species of bushcrickets (Tettigoniidae, Orthoptera). *R. Soc. Open Sci.* **2**, 140473 (2015).
42. P. Cummings, X. Feng, "Domain decomposition methods for a system of coupled acoustic and elastic Helmholtz equations" in *Eleventh International Conference on Domain Decomposition Methods*, C.-H. Lai, P. E. Bjørstad, M. Cross, O. B. Widlund, Eds. (Domain Decomposition Press, Bergen, Norway, 1999), pp. 205–213.
43. COMSOL Multiphysics, Version. 5.5. https://www.comsol.com/. Accessed 12 April 2020.
44. K. J. Bathe, A. Iosilevich, D. Chapelle, An evaluation of the MITC shell elements. *Comput. Struct.* **75**, 1–30 (2000).
45. R Core Team, R: A language and environment for statistical computing, Version 4.0.0 (R Foundation for Statistical Computing, Vienna, Austria, 2020).
46. R. Lenth, EMMEANS: Estimated marginal means, aka least-squares means. R package version 1.5.3. https://CRAN.R-project.org/package=emmeans.